LANGMUIR

pubs.acs.org/Langmuir Article

Molecular Dynamics Study of Bubble Nucleation on a Substrate with Nonuniform Wettability

Yujie Chen, Bing-Nan Chen, Bo Yu,* Wenquan Tao, and Yu Zou

Cite This: *Langmuir* 2020, 36, 5336−5348 Read Online

ACCESS | Metrics & More | Article Recommendations

ABSTRACT: In the present study, the molecular dynamics simulation method is adopted to study bubble nucleation on a platinum substrate with nonuniform wettability. The central region of the substrate has strong hydrophilicity and both sides have weak hydrophobicity. It is interesting that the bubble nucleation happens in the hydrophobic region when the substrate temperature is low, and the nucleation position moves to the hydrophilic region with the increase of the substrate temperature. The intrinsic regime for the change of nucleation position with the substrate temperature is fully illustrated based on the competition between the suffered potential restriction and the absorbed thermal energy of liquid atoms. When the liquid atoms on one region obtain enough thermal energy to break their potential barrier, they convert into a bubble nucleus. Both the potential barrier for liquid atoms clinging to the substrate surface and the solid−liquid heat transfer efficiency improve with the enhancement of substrate hydrophilicity. The potential barrier is decided only by the atomic distribution and interatomic interaction. However, the substrate temperature changes the absorbed thermal energy of the liquid atoms within a specific time, causing the movement of the nucleation position. Furthermore, a hydrophilic nanostructure is introduced to replace the central smooth hydrophilic region and promote lateral heat transfer to the liquid on the hydrophobic region, leading to the improvement of the bubble nucleation efficiency.

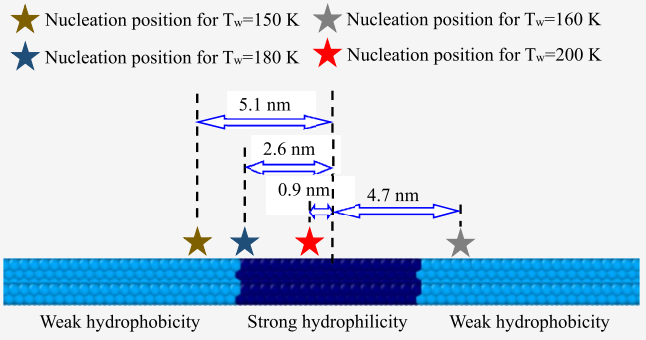

INTRODUCTION

When nucleate boiling occurs on the cooled surface, a large amount of heat will be taken away under the effects of the latent heat of gasification and the disturbance of the departing bubble. Therefore, nucleate boiling has become one of the most efficient ways to cool electronic devices. Wettability is a morphological characteristic of the substrate surface and one of the critical factors in increasing the heat transfer of nucleate boiling.[1−3] Bourdon et al.[4] investigated the effects of wettability on the boiling onset. It was found that wettability variation at the nanoscale triggered the boiling and reduced the substrate superheat. A reduction of at least 3 °C was measured, and the bubble occurred only on the hydrophobic grafted regions, which were patterned on the smooth substrate. Similar conclusions were obtained by Kumar et al.[5] Hsu et al.[6] used a copper cylinder with a mixed wettability of super hydrophilicity and hydrophobicity to study pool boiling. The results showed that more bubbles formed at the interlaced lines of different wetting regions, leading to a reduction of wall superheat and an increase in the efficiency of heat transfer. Chang, Wang, and Bourdon et al.[7−9] also showed that the application of a mixed wettability of hydrophilicity and hydrophobicity could increase the heat transfer performance. Bertossi et al.[10] combined the advantages of hydrophilicity and hydrophobicity to study pool boiling. Results showed that the hydrophobic regions initiated bubble nucleation easily, while hydrophilic ones facilitated bubble detachment. Moreover, the hydrophobic regions provided a bigger nucleation density in comparison to the homogeneous wetting substrate.[5]

However, due to the limitations of spatial scale and time scale, the traditional experimental method cannot adequately reveal the bubble nucleation mechanism, which limits the further development and application of nucleate boiling in enhancing heat transfer. The essence of solid−liquid interfacial wettability is the interaction between solid and liquid particles. The molecular dynamics simulation method (MD) is an available tool to describe the interaction between different particles and the microscopic bubble nucleation process. It has become a popular tool to study the effects of solid−liquid interfacial wettability on phase transitions with the development of

Received: March 17, 2020
Revised: April 24, 2020
Published: April 26, 2020

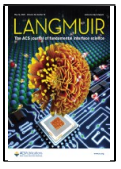

https://dx.doi.org/10.1021/acs.langmuir.0c00747
Langmuir 2020, 36, 5336−5348

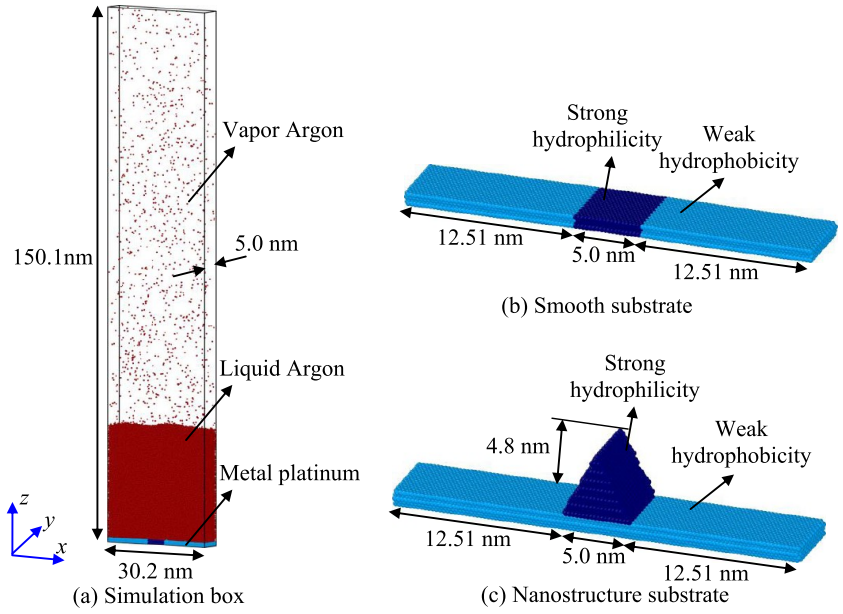

Figure 1. Configurations of (a) simulation box, (b) smooth substrate, and (c) nanostructure substrate.

computer technology.[11] Cao et al.[12] investigated the phase transition of liquid films on a substrate with different wettabilities. The thermal resistance of solid−liquid interface under different wettability conditions was analyzed by the matching degree of the vibrational density of states between the metal atoms and the liquid atoms, and the advantage of the hydrophilic substrate in heat transfer was verified. Shavik et al.[13] analyzed the effects of solid−liquid interfacial wettability on evaporation and explosive boiling, which occurred on a smooth substrate with low and high degrees of temperatures, respectively. The intensity of phase transitions was improved with the increase of substrate hydrophilicity. Similar conclusions were obtained by Hens et al.[14] Wang et al.[15] also studied the effect of substrate wettability on explosive boiling of liquid films. It was found that the explosive boiling tended to occur on the hydrophobic substrate when the heating temperature was low. This was different from the studies of Shavik and Hens because the substrate superheat was much higher in the latter. On the other hand, it was strange that the violent phase transition erupted inside the liquid film after it was lifted away from the hydrophobic substrate. For the hydrophobic substrate, only less thermal energy was transferred to the liquid film after explosive boiling because of the large thermal resistance of the gas film. Wu et al.[16] studied explosive boiling on substrates with uniform and mixed wettability conditions. A gas film was formed between the liquid film and the substrate after explosive boiling, but the substrate surface was still covered with a microfluidic layer. The microfluidic layer thickened with the enhancement of substrate hydrophilicity and was conducive to heat transfer, but the evaporation rate of the liquid film was reduced. Therefore, a substrate with mixed wettability was introduced to reconcile the efficiencies of heat transfer and evaporation rate.

On the other hand, nonuniform wettability plays a critical role in bubble nucleation, which is the initial stage of nucleate boiling and is vital to the enhancement of heat transfer efficiency. Yamamoto et al.[17] investigated the effects of nonuniform wettability and superheat on bubble nucleation. The liquid atoms on the local heater absorbed more thermal energy than those on the cooling region, leading to the formation of bubble nucleation on it. The heat transfer efficiency of the strongly hydrophilic region was much higher than those of the surrounding regions, and its effect was similar to a local heater. As a result, a bubble nucleus was generated on the strongly hydrophilic region. Chen et al.[18] studied the effect of wettability configurations on bubble nucleation on a smooth substrate with a temperature of 200 K. Bubble nucleation was observed on the more hydrophilic region, and the reason for this was illustrated by the temperature trends of liquid atoms on different wetting regions. Furthermore, some common nanostructured substrates with nonuniform wettability were examined to study their effects on bubble nucleation.[19,20] Results showed that the nanostructure provided a larger solid−liquid heat transfer area and promoted bubble nucleation. Zhou et al.[21] explored bubble nucleation on a substrate with nonuniform wettability at different substrate temperatures. The nucleation position appeared in the hydrophobic region and moved to the hydrophilic region with the increase of substrate temperature. The reason for the change of nucleation position was analyzed by the changing trends of heat flux and state points of argon during the bubble nucleation processes. Moreover, the effect of the area fraction of the hydrophobic part on the bubble nucleation temperature was revealed.

Although the above studies have provided significant insights into the bubble nucleation on a substrate with different wettability configurations, the intrinsic regime for this has not been sufficiently revealed yet. It is one-sided to explain the bubble nucleation phenomenon through the difference of the heat transfer efficiency between the liquid and different wetting regions because the potential barrier for bubble nucleation on different wetting regions is different as well. Therefore, in the present study, a smooth substrate having both strong hydrophilicity and weak hydrophobicity is used to study bubble nucleation on it at different substrate temperatures, and the intrinsic regime for bubble nucleation is explained based on the effects of substrate wettability on the heat transfer efficiency and potential barrier. Furthermore, based on the intrinsic regime, the smooth hydrophilic region is replaced with a hydrophilic nanostructure to improve the bubble nucleation efficiency.

https://dx.doi.org/10.1021/acs.langmuir.0c00747
Langmuir 2020, 36, 5336−5348

SIMULATION SYSTEM AND METHOD

As shown in Figure 1a, the simulation system is a cubic box with a size of 30.2 nm (x) × 5.0 nm (y) × 150.1 nm (z), including vapor argon (Ar), liquid argon, and a metal platinum (Pt) substrate. The substrate with five layers of platinum atoms is arranged at the bottom with face-centered cubic structures (fcc (111)). As shown in Figure 1b,c, smooth and nanostructured substrates with nonuniform wettability are constructed in the present study. In these two types of substrates, the central dark blue region has strong hydrophilicity, and the remaining pale blue regions have weak hydrophobicity. The metal substrate is set as the heat source, whose temperature is controlled by a Langevin thermostat. About 97 000 liquid argon atoms are placed on the substrate surface with an initial density of 1.367 g/cm^3. A periodic boundary is applied to the x-direction and the y-direction, and a reflecting wall is applied to the z-direction.

The interaction potentials of Ar−Ar and Pt−Pt are described by the Lennard-Jones (L-J) potential

$$\phi_{\mathrm{Ar-Ar}}(r) = 4\varepsilon_{\mathrm{Ar-Ar}}\left[\left(\frac{\sigma_{\mathrm{Ar-Ar}}}{r}\right)^{12} - \left(\frac{\sigma_{\mathrm{Ar-Ar}}}{r}\right)^{6}\right] \quad (1)$$

$$\phi_{\mathrm{Pt-Pt}}(r) = 4\varepsilon_{\mathrm{Pt-Pt}}\left[\left(\frac{\sigma_{\mathrm{Pt-Pt}}}{r}\right)^{12} - \left(\frac{\sigma_{\mathrm{Pt-Pt}}}{r}\right)^{6}\right] \quad (2)$$

where ε and σ express the energy parameter and length parameter, respectively. The values of these parameters are listed in Table 1.

Table 1. Lennard-Jones Parameters for Ar−Ar and Pt−Pt[22]

interaction type	ε (eV)	σ (nm)
Ar−Ar	0.0104	0.3405
Pt−Pt	0.5219	0.2475

The interaction potential of Ar−Pt is related to the solid−liquid interfacial wettability, and a modified L-J potential is adopted.[22]

$$\phi_{\mathrm{Ar-Pt}}(r) = 4\varepsilon_{\mathrm{Ar-Pt}}\left[\left(\frac{\sigma_{\mathrm{Ar-Pt}}}{r}\right)^{12} - \beta\left(\frac{\sigma_{\mathrm{Ar-Pt}}}{r}\right)^{6}\right] \quad (3)$$

$$\varepsilon_{\mathrm{Ar-Pt}} = \alpha\sqrt{\varepsilon_{\mathrm{Ar}}\varepsilon_{\mathrm{Pt}}} \quad (4)$$

$$\sigma_{\mathrm{Ar-Pt}} = \frac{\sigma_{\mathrm{Ar}} + \sigma_{\mathrm{Pt}}}{2} \quad (5)$$

where $\varepsilon_{\mathrm{Ar-Pt}}$ and $\sigma_{\mathrm{Ar-Pt}}$ are calculated based on the Lorentz−Berthelot combining rule.[23] α and β are the key parameters to adjust the solid−liquid interfacial wettability, and their values are illustrated in Table 2.

Table 2. Different Wetting Substrates Based on α and β[22]

wettability	α	β	contact angle (deg)
strong hydrophilicity	1.0	1.0	0
weak hydrophobicity	0.14	0.5	95

The present study is conducted using the Large-Scale Atomic/Molecular Massively Parallel Simulator (LAMMPS).[24] During the simulation process, the potential energy on each atom is calculated by the L-J potential within a cutoff radius of 3.5$\varepsilon_{\mathrm{Ar}}$ every 5 fs, and the position and velocity of each atom are updated by the velocity-Verlet algorithm.[25] The simulation procedure is illustrated as follows: first, a 2.5 ns equilibrium simulation at a temperature of 90 K is conducted in the canonical ensemble (NVT); then, the substrate temperature is raised to 145, 150, 160, 180, and 200 K to study the effects of substrate temperature on bubble nucleation, and another 25.0 ns nonequilibrium simulation is conducted in the microcanonical ensemble (NVE). It is noteworthy that the simulation procedure in the case with a smooth substrate is the same as that in the case with a nanostructure substrate.

RESULTS AND DISCUSSION

Based on the above simulation systems and methods, the bubble nucleation on a smooth substrate with nonuniform wettability at different temperatures is studied and the intrinsic regime for this is illustrated. Furthermore, a nanostructure substrate with nonuniform wettability is constructed to improve the nucleation efficiency based on the intrinsic regime.

Explosion of Bubble Nucleation on a Smooth Substrate with Nonuniform Wettability at Different Temperatures. It has been found that the substrate temperature has a significant impact on MD studies of phase transitions.[13,21] Therefore, the representative temperature values of 145, 150, 160, 180, and 200 K are selected to investigate their effects on bubble nucleation. Figure 2 illustrates the representative snapshots of the phase transition processes on the smooth substrates with different temperatures. The initial moment of nonequilibrium simulation is 2500 ps. Only evaporation occurs on the smooth substrate with a temperature of 145 K within 27 500 ps. When the substrate temperature is higher than 150 K, a visible bubble nucleus turns up on the substrate and is marked with a red ring. However, the nucleation position is different at different substrate temperatures. When the substrate temperature is 150 or 160 K, the nucleation position is on the hydrophobic region, as shown in Figure 2b,c. With the increase of substrate temperature, the nucleation position moves closer to the hydrophilic region and finally stays on the center of the hydrophilic region, as shown in Figure 2d,e. The simulation results on the smooth substrate with nonuniform wettability are similar to the experimental results of Bourdon et al.,[4] which show that a lower superheat is needed for bubble nucleation on the hydrophobic region. The reason for the change of nucleation position is illustrated in the following parts.

As shown in Figure 3, to conveniently explain the intrinsic regime of the change of nucleation position at different substrate temperatures, based on the nucleation positions in Figure 2, the liquid in the vicinity of the substrate is divided into four regions: Region 1 on the hydrophilic region, Region 2 on the border of the hydrophilic region and hydrophobic region, Region 3 on the hydrophobic region, and Region 4 on top of Region 1.

On the nanoscale, the difference between a group of vapor atoms and liquid atoms is that the former move within a bigger space than the latter. The L-J atom has only two types of energy: kinetic energy and potential energy. The statistical average value of the atomic kinetic energy is the temperature, which is the motive force for bubble nucleation. On the other hand, the potential energy poses a movement limitation on liquid atoms and corresponds to the potential barrier for bubble nucleation. If the liquid atoms in the vicinity of the substrate obtain enough kinetic energy to break their potential restriction, bubble nucleation occurs.[26] Therefore, next, the effects of substrate wettability on potential restriction and the solid−liquid heat transfer efficiency are discussed.

https://dx.doi.org/10.1021/acs.langmuir.0c00747
Langmuir 2020, 36, 5336−5348

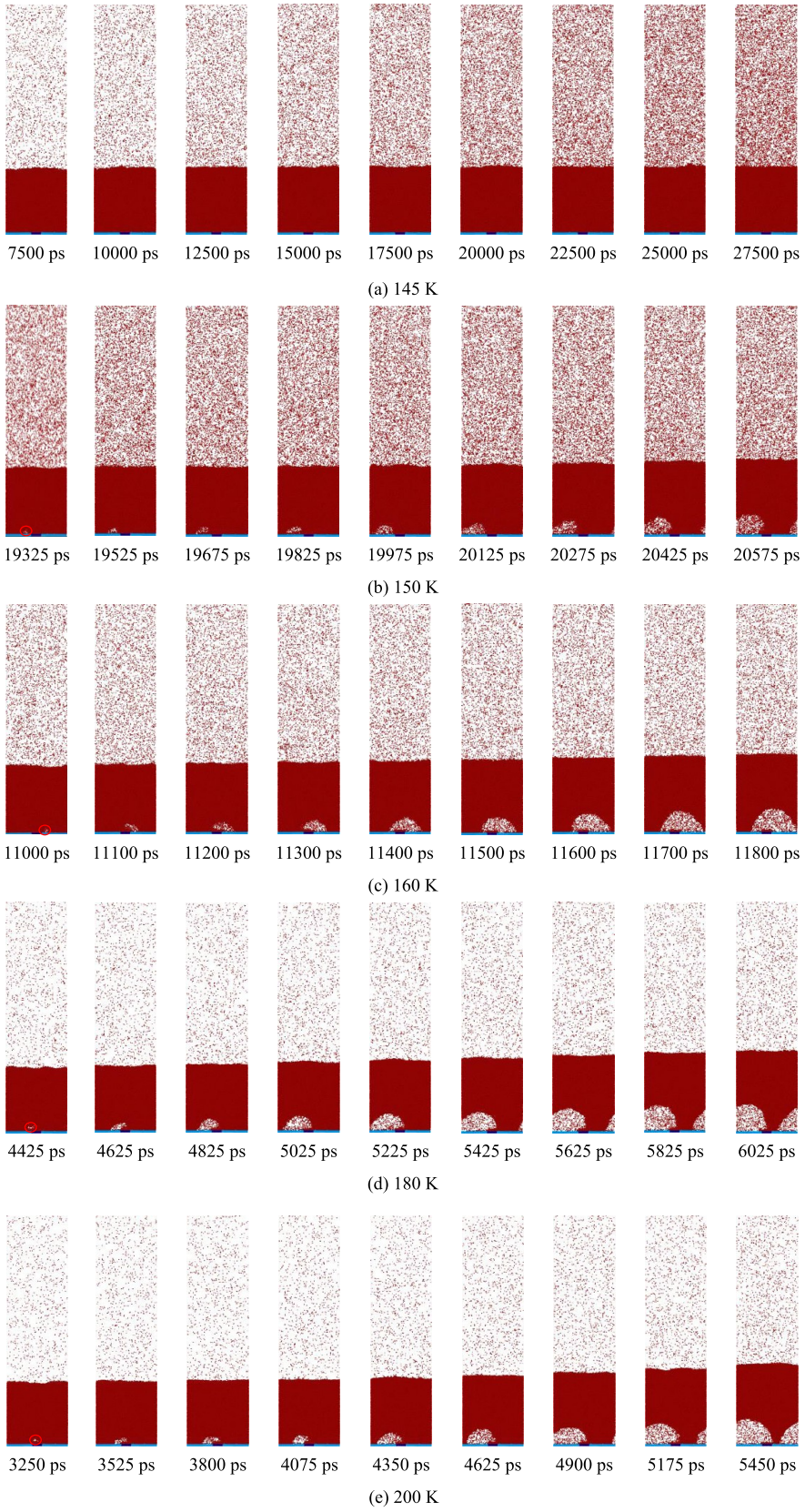

Figure 2. Representative snapshots of phase transition processes on the smooth substrates at (a) 145, (b) 150, (c) 160, (d) 180, and (e) 200 K.

First, the effects of substrate wettability on potential restriction for bubble nucleation are discussed. The potential restriction on liquid atoms is related to the atomic distribution and interaction potential. The Lennard-Jones potential is used to describe the interaction between different atoms in the present study, and it is independent of the simulation processes. However, liquid atoms become more vigorous after absorbing thermal energy from the substrate during the nonequilibrium

https://dx.doi.org/10.1021/acs.langmuir.0c00747
Langmuir 2020, 36, 5336−5348

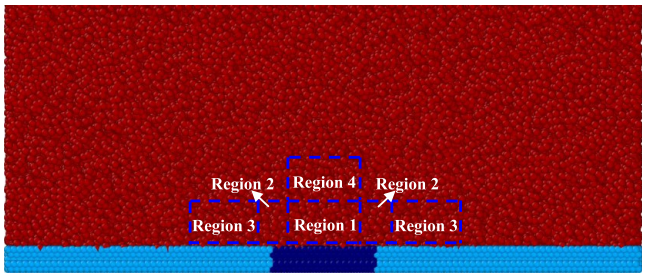

Figure 3. Diagrammatic sketch of the division of region for the illustration of bubble nucleation difference.

simulation stage, and the distance between different liquid atoms is increased, leading to a change of atomic distribution. The potential restriction on liquid atoms is weakened with the increase of atomic distance. In the present study, the substrate temperatures of 145, 150, 160, 180, and 200 K are used to study their effects on bubble nucleation. The liquid atoms on the substrates with different temperatures absorb different thermal energies within the same time. Therefore, the distribution of potential energy is illustrated at the initial moment of the nonequilibrium simulation, as shown in Figure 4 (z = 0 Å is the

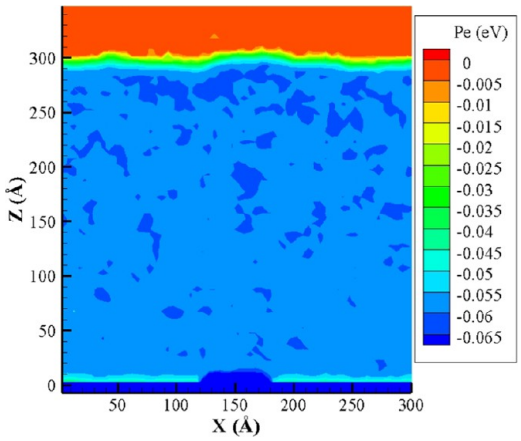

Figure 4. Contour of potential energy in the case of a smooth substrate at the initial moment of the nonequilibrium simulation.

position of the solid−liquid interface). The value of potential energy is negative, indicating that the potential energy is a restriction on the atomic movement (the absolute value of potential energy is the potential restriction on liquid atoms). It is evident that the potential restriction on the liquid atoms is much larger than that on the vapor atom. Therefore, the liquid atoms cannot but preserve their phase state before obtaining enough thermal energy from the substrate. For the liquid atoms in the vicinity of the substrate, their suffered potential restriction is different under the effect of different solid−liquid interfacial wettabilities. The potential restriction on liquid atoms in Region 3 is much weaker than that in Region 1, and it is even weaker than that on the atoms totally inside the liquid region (Region 4). For the liquid atoms in Region 2, the magnitude of potential restriction is between the magnitude on the liquid atoms in Region 1 and that in Region 3. It is worth stressing that the approximate influence range of large potential restriction from the hydrophilic region on liquid atoms is within 3.3 nm from the center of the hydrophilic region and liquid atoms in Region 3 are out of the influence range. Obviously, considering only the effect of wettability on the heat transfer to explain bubble nucleation on a smooth substrate with nonuniform wettability is one-sided.

The second is about the effects of substrate wettability on the solid−liquid heat transfer efficiency, and it is worth stressing that the analysis focus of heat transfer is on the liquid close to the substrate. The simulation case with the representative substrate temperature of 150 K is taken to illustrate the laws of heat transfer during the nonequilibrium heating process. Figure 5 shows the temperature contours at some representative time steps. The temperature distribution is approximately uniform at 2500 ps, which is the initial moment of the nonequilibrium simulation. It is noteworthy that the scattered vapor atoms cause a statistical error of temperature and some points with a high-temperature value in the upper vapor region. Then, the substrate temperature is raised to 150 K, and the liquid atoms begin to absorb thermal energy from the substrate. At 2600 ps, the temperature of the liquid atoms in Region 1 increases obviously, but no noticeable change of temperature occurs in Region 3, as shown in Figure 5b. This difference indicates that the solid−liquid heat transfer efficiency in the hydrophobic region is much lower than that in the hydrophilic region. Kapitza resistances of 1.89×10^{-8} and 185.35×10^{-8} K·m^2/W are obtained for the strongly hydrophilic surface and the weakly hydrophobic surface, respectively, by the method in ref 27. The latter is about 98 times bigger than the former. On the other hand, the thermal conductivity of liquid argon is 0.125 W/(m·K),[12] and the thermal resistance of a layer of liquid argon with a thickness of 231.7 nm is equal to the Kapitza resistance of the weakly hydrophobic region. Therefore, it is hard for the liquid atoms in Region 3 to obtain thermal energy from the hydrophobic region. As time progresses, the liquid atoms in Region 1 continue to increase their temperature. Meanwhile, the temperature difference between the liquid atoms in Region 1 and Regions 2, 3, and 4 becomes larger and larger. As a result, a momentum exchange occurs, and the temperatures of the liquid atoms in Regions 2, 3, and 4 are significantly increased at 2800 ps, as shown in Figure 5c. Finally, at 7500 ps, the temperature of liquid atoms on the hydrophobic region is raised to about 115 K by the liquid−liquid transversal heat transfer, as shown in Figure 5d.

The thermal energy exchange between the liquid atoms in Region 1 and those in Regions 2 and 3 is the focus in the explanation of nucleation position change. Therefore, to more intuitively illustrate transversal heat transfer from the liquid atoms in Region 1 to those in Regions 2 and 3, two domains with a size of 20 Å (x) × 20 Å (z) at the border of the hydrophilic and the hydrophobic regions are set to calculate the transversal heat flux, as shown in Figure 6. The heat fluxes through these two regions are illustrated in Figure 7. During the simulation process, the rightward and leftward heat fluxes are smaller and bigger than 0, respectively, indicating that some thermal energy is transferred from the liquid atoms on the hydrophilic region to those on the hydrophobic region. Therefore, the evolution law of temperature in Figure 5 is quantitatively verified.

On the other hand, although an equilibrium state at 90 K is obtained after 2.5 ns equilibrium simulation in the present study, the temperature distribution is not absolutely uniform at the initial moment of the nonequilibrium simulation stage because of the atomic irregular movement and distribution, as shown in Figure 5a. Moreover, the potential restriction on each atom is related to the atomic distribution, and it is also not absolutely uniform at the initial moment of the nonequilibrium simulation stage, as shown in Figure 4. As a result, although the simulation system is symmetric in the x-direction, the absorbed thermal

https://dx.doi.org/10.1021/acs.langmuir.0c00747
Langmuir 2020, 36, 5336−5348

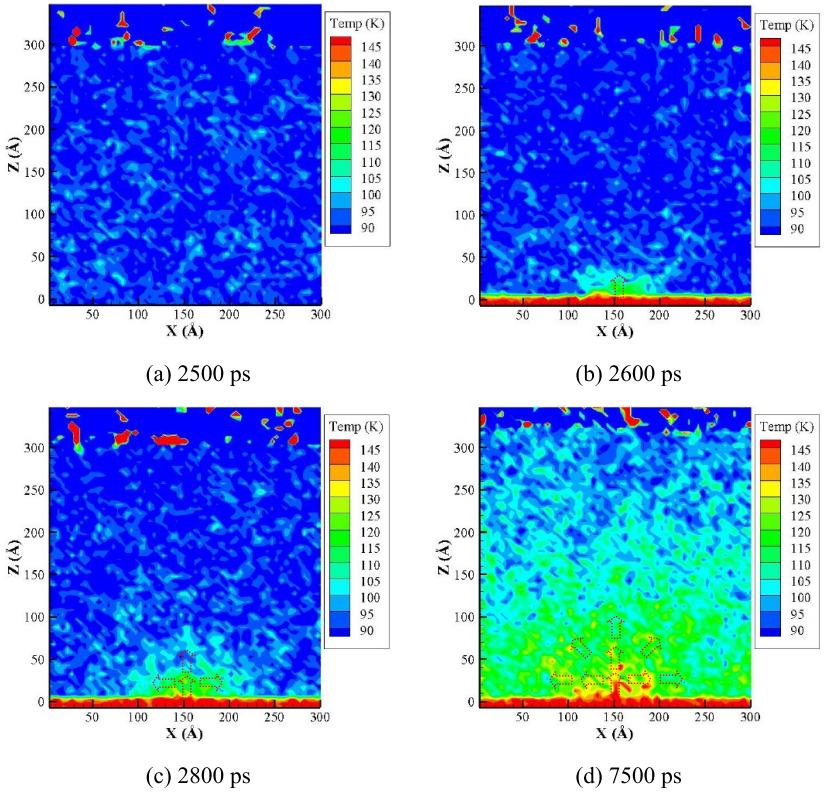

Figure 5. Contour of temperature in the case of a smooth substrate at 150 K at (a) 2500, (b) 2600, (c) 2800, and (d) 7500 ps.

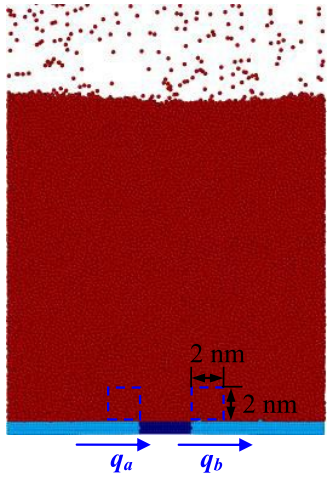

Figure 6. Diagrammatic sketch of the computational region for heat flux.

energy of liquid atoms on the symmetric hydrophobic regions has small differences during the nonequilibrium simulation stage. Therefore, the nucleation position may prefer one side or both sides of the smooth substrate when the substrate temperature is low, but we cannot know it in advance. The average values of heat flux q_a and q_b are -0.16×10^{-4} and 0.12×10^{-4} eV/Å^2·ps, respectively. The rightward heat flux is smaller than the leftward heat flux. To some extent, this explains why the nucleation position is at the left side of the substrate when the substrate temperature is 150 K.

Furthermore, to conveniently explain the intrinsic regime for the change of the nucleation position at different substrate temperatures, combined with the nucleation time in Figure 2, the heat transfer process is approximately divided into three main stages: the longitudinal heat transfer stage, the initial transversal heat transfer stage, and the full-scale transversal heat transfer stage. The liquid in Region 1 absorbs a large amount of thermal energy from the hydrophilic region in the longitudinal heat transfer stage (2500−3250 ps). Then, the liquid in Region 2 absorbs a considerable amount of thermal energy from the liquid in Region 1 in the initial transversal heat transfer stage (3255−4425 ps). Furthermore, a great amount of thermal energy from the liquid in Region 2 is transferred to that in Region 3 in the full-scale transversal heat transfer stage (4425 ps). In these three stages, the liquid atoms in Regions 1−3 try to convert into a bubble nucleus. It is noteworthy that the thermal energy exchange occurs between different atoms everywhere during the whole simulation process, and the division of the heat transfer stage depends on the leading process of thermal energy exchange. On the other hand, the liquid on the hydrophobic region also absorbs thermal energy from the substrate, but it is almost negligible compared to the thermal energy from the liquid on the hydrophilic region.

Based on the above analyses, we find that the potential restriction on the liquid atoms clinging to the substrate increases with the improvement of substrate hydrophilicity. However, the thermal energy from the substrate flows through the liquid on the hydrophilic region to the liquid on the hydrophobic region, and Region 1 is the first arrival position of heat flow, followed by Regions 2 and 3. Therefore, it is hard to explain the change of the nucleation position so far.

The potential restriction from different wetting regions to the liquid atoms is related only to the atomic distribution and interatomic interaction. However, the absorbed thermal energy of the liquid within a specific time improves with the increase of the substrate temperature. If the thermal energy that flows into Region 1 in the longitudinal heat transfer stage is large enough to

https://dx.doi.org/10.1021/acs.langmuir.0c00747
Langmuir 2020, 36, 5336−5348

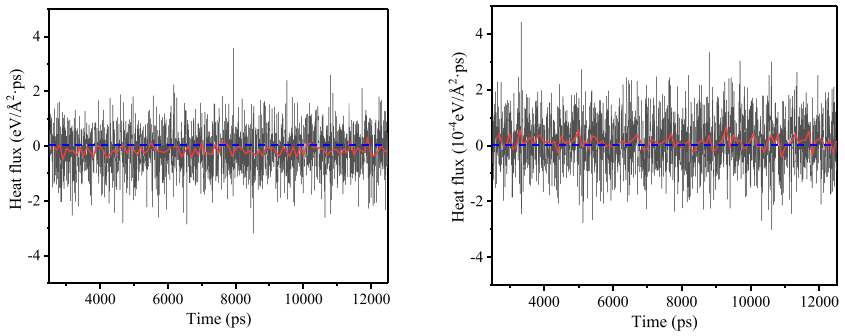

(a) Leftward heat flux (b) Rightward heat flux

Figure 7. Transversal heat transfer through the regions at the border of the smooth hydrophilic region and the smooth hydrophobic region: (a) leftward heat flux and (b) rightward heat flux.

break the potential restriction, a bubble nucleus forms in Region 1. If not, Regions 2 and3 are checked in turn in the transversal heat transfer stages. Therefore, at different substrate temperatures, further comparison between the average kinetic energy and the average potential restriction is made to clarify the intrinsic regime for the change of the nucleation position. It is worth stressing that temperature is associated with atomic average kinetic energy, and the latter is more suitable to make a comparison with the average potential restriction, as shown in eq 6

$$\overline{\varepsilon_K} = \frac{\sum 1/2 m_i v_i^2}{N} = 3/2kT \tag{6}$$

where $k = 1.380649 \times 10^{-23}$ J/K is the Boltzmann constant.

Figure 8 shows the contours of kinetic energy, potential energy, and total energy in the cases with smooth substrates at different temperatures at 3250 ps, which is the end moment of the longitudinal heat transfer stage. After increasing the substrate temperature to a high value, the liquid atoms in Region 1 absorb a large amount of thermal energy from the substrate to increase their kinetic energy quickly. One part of thermal energy is converted to atomic potential energy, and the potential restriction on liquid atoms is weakened. Meanwhile, the liquid atoms in Region 2 obtain a small amount of thermal energy to increase their kinetic energy and weaken their potential restriction. As shown in the kinetic energy contours in Figure 8, the liquid atoms in Region 1 obtain more kinetic energy with the increase of substrate temperature. Moreover, the violent movement of liquid atoms in Region 1 leads to a significant attenuation of potential restriction for bubble nucleation, especially for the case with a substrate temperature of 200 K, as shown in the potential energy contours in Figure 8. As a result, for the substrate with a temperature of 200 K, the liquid in Region 1 obtains a large amount of kinetic energy to break its potential restriction and convert into a bubble nucleus on the central hydrophilic region at 3250 ps, as shown in the total energy contour in Figure 8d. However, for the cases with a lower substrate temperature than 180 K, the substrate cannot offer enough thermal energy for the liquid atoms in Region 1 to break their potential restriction in the longitudinal heat transfer stage, and no bubble nucleation occurs.

Figure 9 illustrates the temperature trend of a layer of liquid atoms clinging to the surface of the strongly hydrophilic region at 200 K, which increases quickly to a temperature close to the substrate temperature of 200 K after 2750 ps. The temperature trend indicates that an approximate equilibrium of thermal energy exchange appears between the hydrophilic region and this layer of liquid atoms, which cannot increase their kinetic energy further. However, the potential restriction on the liquid atoms clinging to the strongly hydrophilic region is so strong that they cannot get rid of it, as shown in Figure 8. The highest substrate temperature is 200 K in the present study. Therefore, for all cases in the present study, the surface of the strongly hydrophilic region is still covered by a layer of liquid atoms after bubble nucleation.

As time progresses, the intensity of the thermal energy exchange between the liquid atoms in Region 1 and the hydrophilic region becomes weaker because of the small temperature difference. The thermal energy exchange between the liquid atoms in Region 2 and those in Region 1 takes dominance, and the initial transversal heat transfer stage is reached. As shown in Figure 10, the liquid atoms in Region 2 obtain a large amount of thermal energy from those in Region 1 to improve their kinetic energy and weaken their potential restriction in the initial transversal heat transfer stage. For the case with a substrate temperature of 180 K, although the liquid in Region 1 cannot convert into a bubble nucleus in the longitudinal heat transfer stage, it has a strong capacity to transfer thermal energy to the liquid in Region 2. On the other hand, potential restriction on the liquid atoms in Region 2 is weaker than that in Region 1. As a result, the liquid atoms in Region 2 get rid of their potential restriction, and a bubble nucleus appears in Region 2 at 4425 ps. However, for the cases with substrate temperatures of 160 and 150 K, the liquid atoms in Regions 1 and 2 need more time to weaken the potential restriction on them, and no bubble nucleation phenomenon occurs in the initial transversal heat transfer stage.

As the heating process continues, more and more thermal energy exchanges between the liquid atoms in Region 2 and those in Region 3 take place during the full-scale transversal heat transfer stage. In this stage, the liquid atoms in Regions 1, 2, and 3 absorb thermal energy to weaken their potential restriction for bubble nucleation simultaneously. However, the liquid atoms in Region 3 suffer the weakest potential restriction, and they tend to convert into a bubble nucleus first in the full-scale transversal heat transfer stage, as shown in Figure 11. For the case with a substrate temperature of 160 K, the liquid atoms in Region 3 obtain more thermal energy than those in the case with a substrate temperature of 150 K within the same time. Therefore, the liquid atoms on the left border of the hydrophobic region break their potential restriction at 11 000 ps in the case with a substrate temperature of 160 K, as shown in Figure 11b. For the case with a low substrate temperature of 150 K, the liquid atoms in Region 3 require more time to obtain enough kinetic energy

https://dx.doi.org/10.1021/acs.langmuir.0c00747
Langmuir 2020, 36, 5336−5348

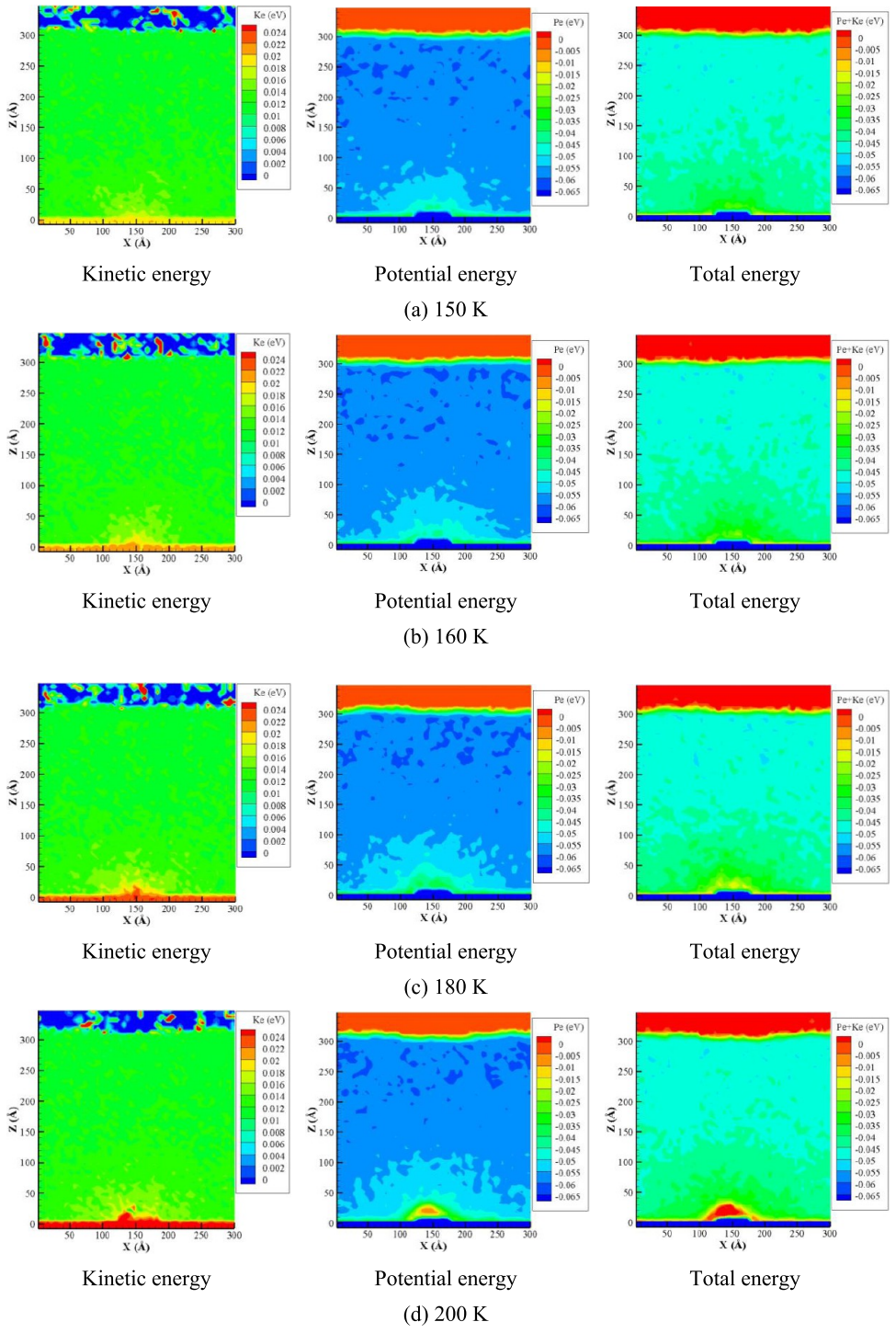

Figure 8. Contours of kinetic energy, potential energy, and total energy in the cases with smooth substrates at (a) 150, (b) 160, (c) 180, and (d) 200 K at 3250 ps.

to break their weak potential restriction and convert into a bubble nucleus at 19 525 ps, as shown in Figure 12. It is worth stressing that the liquid atoms in Region 4 obtain more thermal energy than those in Region 3 before 19 525 ps, but the former suffers more considerable potential restriction, leading to no bubble nucleus formation in Region 4 before 19 525 ps.

On the other hand, the required thermal energy for bubble nucleation on the hydrophobic region is almost the same, which is mainly provided from the hydrophilic region. The liquid atoms in Region 3 absorb more thermal energy than those far from the hydrophilic region within the same time. As a result, when the substrate temperature is low, only the liquid atoms in Region 3 first obtain enough thermal energy to break their potential restriction and convert into a bubble nucleus. The simulation results qualitatively explain the experimental results of Bourdon et al.,[4] which show that a lower superheat is needed for bubble nucleation on the hydrophobic region. Furthermore, a distance of 3.6 nm from the nucleation position to the center of the hydrophilic region is obtained when the substrate temperature is 162 K, and the nucleation position is close to the

https://dx.doi.org/10.1021/acs.langmuir.0c00747
Langmuir 2020, 36, 5336−5348

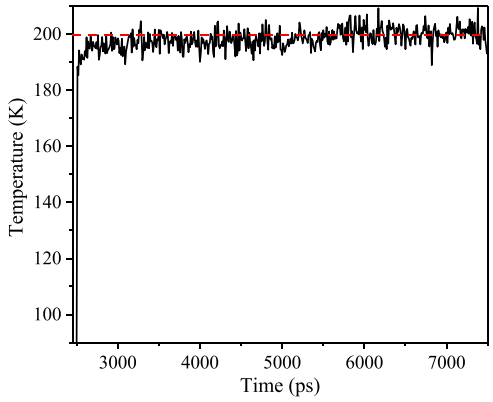

Figure 9. Temperature trend of the liquid clinging to the hydrophilic region in the case of a smooth substrate at 200 K.

influence range (3.3 nm) of the large potential restriction from the hydrophilic region. Therefore, the substrate temperature of 162 K is regarded as the approximate critical temperature for the movement of the nucleation position from Region 3 to Region 2 in the present study. However, when the substrate temperature is raised to 180 K, the liquid atoms in Region 1 still cannot convert into a bubble nucleus, and bubble nucleation occurs in Region 2. Both Regions 2 and 3 are close to the border of the hydrophilic and hydrophobic regions. It can be concluded that the bubble nucleus tends to appear near the border of the hydrophilic region and the hydrophobic region when the substrate temperature is not extremely high. To some extent, this explains why more bubbles form at the interlaced lines of different wetting regions in the experiment of Hsu et al.[6]

In summary, the initial potential restriction on liquid atoms in the vicinity of the substrate only relates to the substrate wettability, but the motive force to break the potential restriction is dependent on the substrate temperature. Thermal energy from the hydrophilic region transfers to the liquid atoms gradually from the proximal segment to the distal segment in three successive stages, corresponding to three nucleation positions with successively reduced potential restriction. Therefore, when the substrate temperature is low, the bubble nucleation occurs only on the hydrophobic region close to the border of the hydrophilic region and hydrophobic region (Region 3). Then, the nucleation position moves closer to the

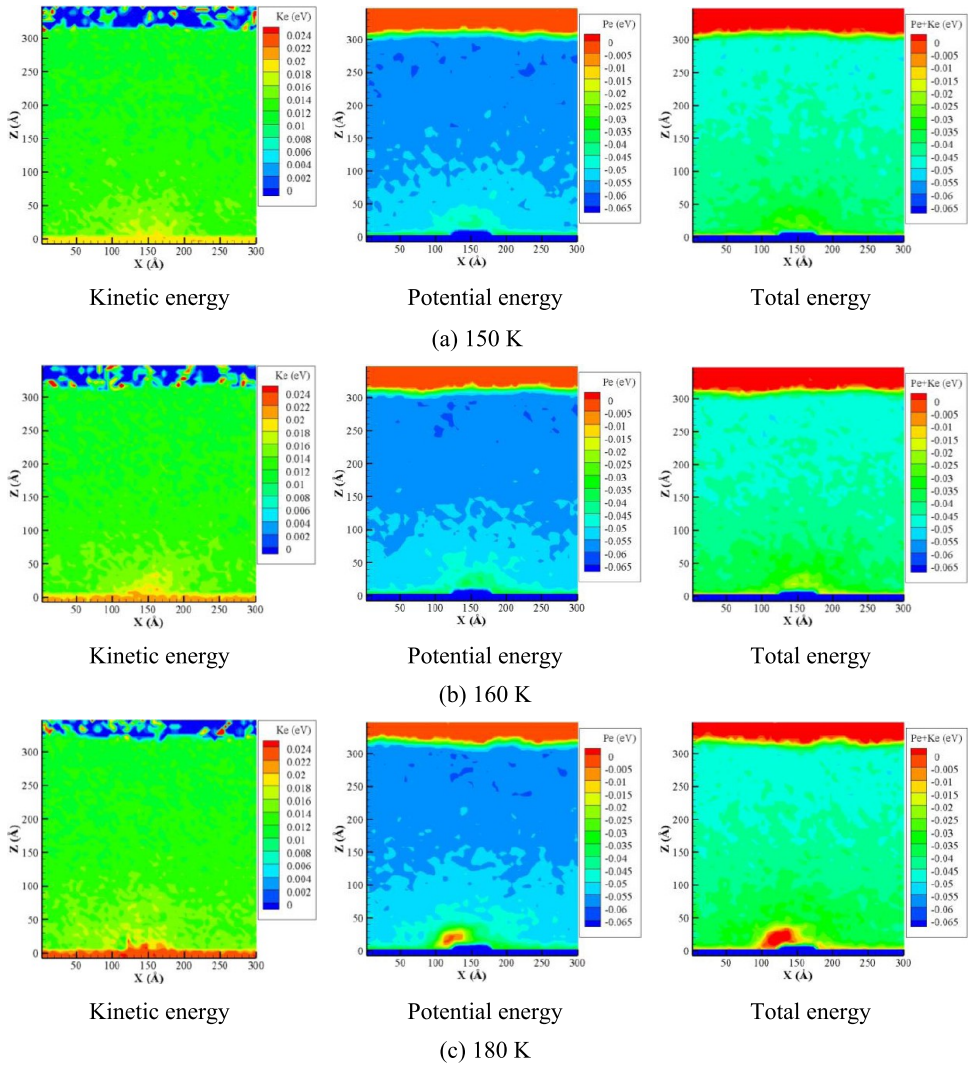

Figure 10. Contours of kinetic energy, potential energy, and total energy in the cases with smooth substrates at (a) 150, (b) 160, and (c) 180 K at 4425 ps.

https://dx.doi.org/10.1021/acs.langmuir.0c00747
Langmuir 2020, 36, 5336−5348

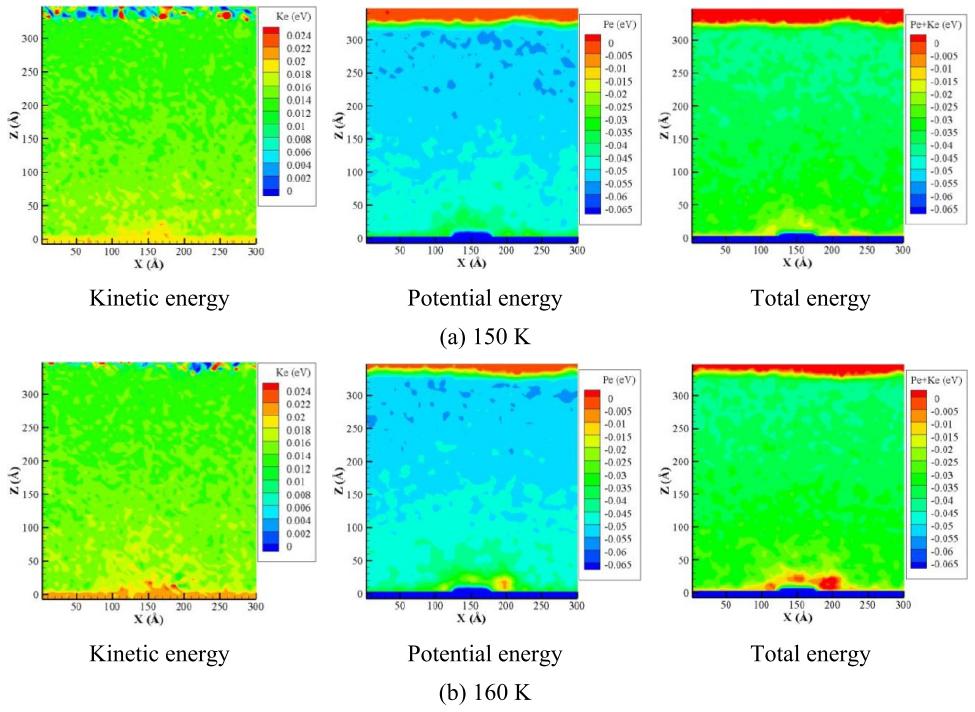

Figure 11. Contours of kinetic energy, potential energy, and total energy in the cases with smooth substrates at (a) 150 and (b) 160 K at 11 000 ps.

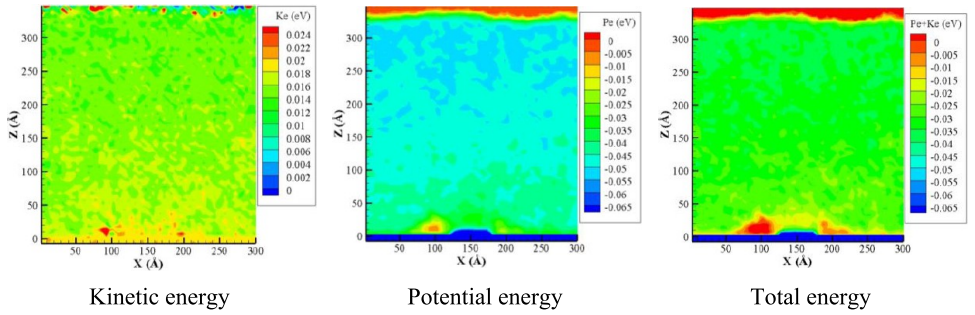

Figure 12. Contours of kinetic energy, potential energy, and total energy in the case with a smooth substrate at 150 K at 19 325 ps.

hydrophilic region when the substrate temperature exceeds a high value of about 162 K.

Explosion of Bubble Nucleation on a Nanostructure Substrate with Nonuniform Wettability at Different Temperatures. It has been found that the liquid atoms on the hydrophobic region suffer less potential restriction than those on the hydrophilic region, but the former obtains the required kinetic energy for bubble nucleation from the latter in the full-scale transversal heat transfer stage. As a result, the bubble nucleation efficiency on the hydrophobic region is at a low level. If the central smooth hydrophilic region is replaced with a convex hydrophilic nanostructure, as shown in Figure 1c, the longitudinal heat transfer stage is passed, and the liquid atoms near the hydrophobic region obtain thermal energy from the hydrophilic nanostructure directly. Moreover, the nanostructure provides a larger solid−liquid heat exchange area. As a result, the bubble nucleation efficiency is improved by the hydrophilic nanostructure. The details are illustrated in the following parts.

Figure 13 shows the representative snapshots of phase transition processes on the nanostructure substrates with different temperatures. It is interesting that a bubble nucleus turns up on the right side of the nanostructure at 7900 ps when the substrate temperature is 145 K but only the evaporation phenomenon occurs on the smooth substrate at 145 K, as shown in Figure 2a. Moreover, the incipient nucleation time on the nanostructure substrate at 145 K is even earlier than that on the smooth substrate at 160 K. Figure 14 shows the comparison between the smooth substrate and the nanostructure substrate in the incipient nucleation time. The incipient nucleation time is significantly shortened by the nanostructure substrate, especially when the substrate temperature is low. On the other hand, there is another phenomenon different from the case with a smooth substrate in which two bubble nuclei form simultaneously on both sides of the nanostructure when the substrate temperature is higher than 160 K, and they finally coalesce with each other.

Then, the nanostructure substrate with a temperature of 150 K is taken as a representative to illustrate the reason for the shortening of the incipient nucleation time by the nanostructure substrate. As shown in Figure 15, for the nanostructure substrate, the potential restriction on liquid atoms on the hydrophobic region is much weaker than that on the hydrophilic nanostructure region at the initial moment of the non-equilibrium stage and so is the potential restriction distribution on the smooth substrate. Therefore, the difference in incipient nucleation time between the smooth substrate and the

https://dx.doi.org/10.1021/acs.langmuir.0c00747
Langmuir 2020, 36, 5336−5348

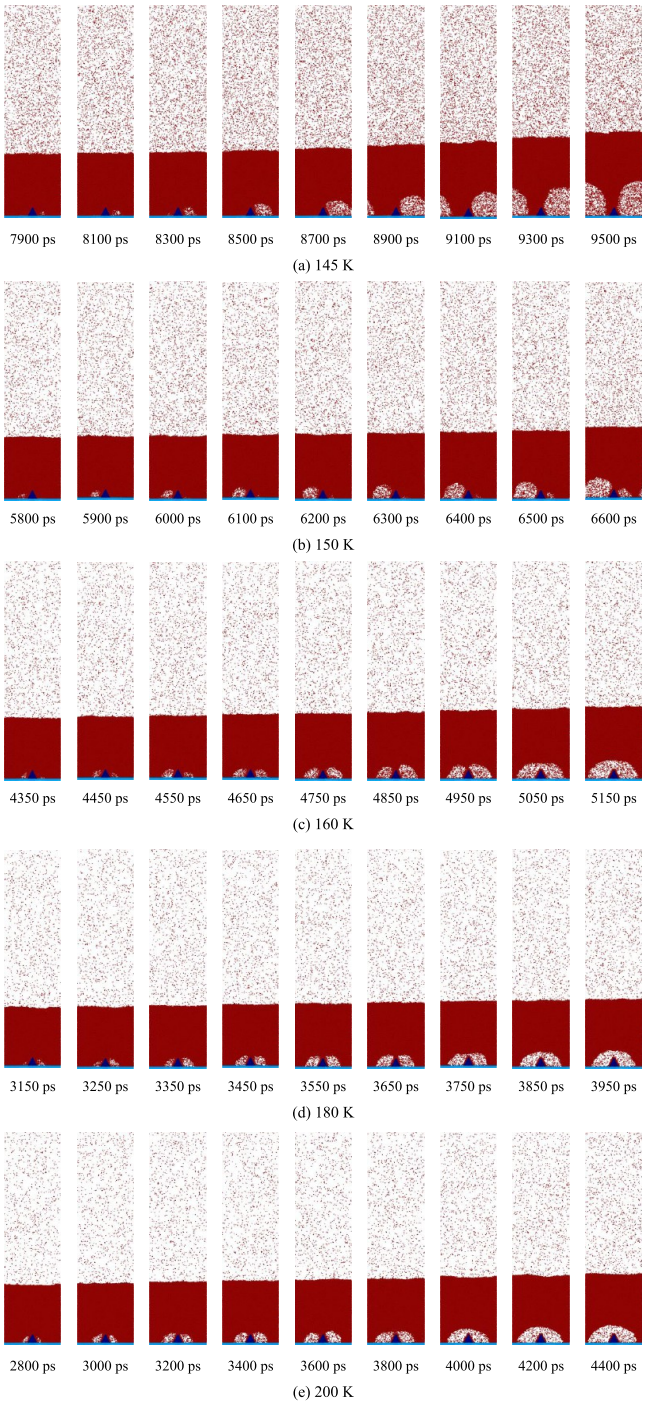

Figure 13. Representative snapshots of phase transition processes on the nanostructure substrates at (a) 145, (b) 150, (c) 160, (d) 180, and (e) 200 K.

nanostructure substrate mainly depends on the heat transfer process. The regions for calculating the transversal heat flux in the case with a nanostructure substrate are the same as that in Figure 6. At the substrate temperature of 150 K, the comparisons of the transversal heat flux through the regions at the border of the hydrophilic region and the hydrophobic region between the smooth substrate and the nanostructure substrate are shown in Figure 16. Obviously, the liquids in Regions 2 and 3 on the nanostructure substrate obtain more thermal energy than those on the smooth substrate within the same time. As a result, the

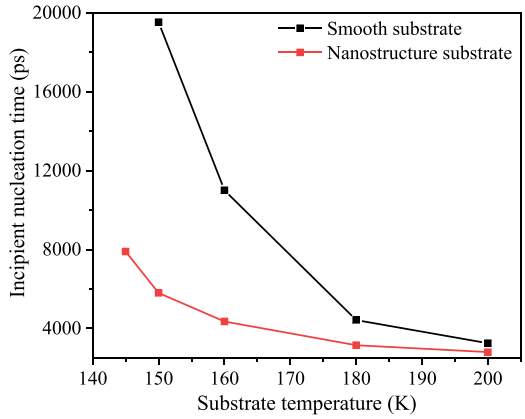

Figure 14. Comparison between the smooth substrate and the nanostructure substrate in the incipient nucleation time.

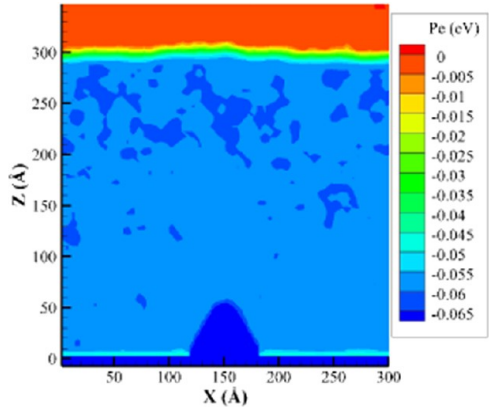

Figure 15. Contour of potential energy in the case with a nanostructure substrate at the initial moment of the nonequilibrium simulation.

incipient nucleation time is significantly advanced by the hydrophilic nanostructure substrate.

CONCLUSIONS

In this article, the molecular dynamics simulation method is adopted to study bubble nucleation on a substrate with nonuniform wettability. The nucleation position is observed to vary with the substrate temperature is observed, and the intrinsic regime for this is fully illustrated. The conclusions are summarized as follows.

For the smooth substrate with nonuniform wettability, the nucleation position is related to the substrate temperature. The bubble nucleus appears on the hydrophobic region when the substrate temperatures are 150 and 160 K. With the increase of substrate temperature, the nucleation position moves forward to the hydrophilic region and finally locates there. The change of the nucleation position is explained through the competition of atomic potential restriction and atomic kinetic energy, which are the barrier and the impetus for bubble nucleation, respectively.

The liquid atoms on the hydrophilic region suffer a stronger potential restriction than those on the hydrophobic region. Therefore, the liquid atoms on the hydrophilic region need to obtain more thermal energy to get rid of their potential restriction and convert into a bubble nucleus. On the other hand, the thermal energy exchange efficiency between the liquid and substrate is related to the solid−liquid interfacial wettability as well. The Kapitza resistance for the hydrophobic region is about

https://dx.doi.org/10.1021/acs.langmuir.0c00747
Langmuir 2020, 36, 5336−5348

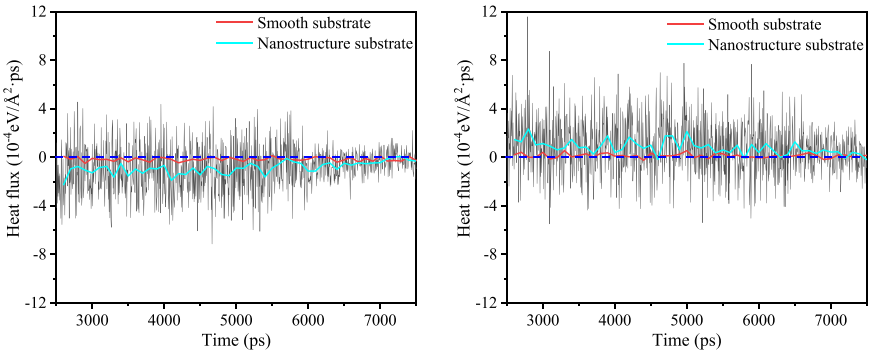

Figure 16. Transversal heat transfer through the regions at the border of the hydrophilic nanostructure and the hydrophobic region: (a) rightward heat flux and (b) leftward heat flux.

98 times larger than that for the hydrophilic region. After increasing the substrate temperature to a high value from the equilibrium temperature of 90 K, only the liquid atoms on the hydrophilic region absorb a considerable amount of thermal energy in a short time, and part of the absorbed thermal energy is further transferred to the liquid atoms on the hydrophobic region. Therefore, although the liquid atoms on the hydrophobic region suffer weak potential restriction, they need more time to obtain the thermal energy to break the weak potential restriction and convert into a bubble nucleus. The magnitude of the absorbed thermal energy of liquid atoms is related to the substrate temperature. As a result, the liquid atoms with a large potential restriction on the hydrophilic region achieve nucleation when the substrate temperature is 200 K, and the nucleation position moves to the hydrophobic region with the decrease of the substrate temperature. Moreover, the bubble nucleation occurs only on the hydrophobic region close to the border of the hydrophilic region and hydrophobic region when the substrate temperature is below 162 K.

Furthermore, the central smooth hydrophilic region is replaced with a convex hydrophilic nanostructure, and the liquid atoms on the hydrophobic region obtain thermal energy from the hydrophilic nanostructure directly. As a result, the bubble nucleation efficiency in the hydrophobic region is improved. The present study can provide a reference for research on enhancing heat transfer.

AUTHOR INFORMATION

Corresponding Author

Bo Yu − *School of Mechanical Engineering, Beijing Key Laboratory of Pipeline Critical Technology and Equipment for Deepwater Oil & Gas Development, Beijing Institute of Petrochemical Technology, Beijing 102617, China;* orcid.org/0000-0002-4231-6914; Phone: +86-10-81292805; Email: yubobox@vip.163.com

Authors

Yujie Chen − *Key Laboratory of Thermo-Fluid Science and Engineering, Ministry of Education, School of Energy & Power Engineering, Xi'an Jiaotong University, Xi'an, Shaanxi 710049, China*

Bing-Nan Chen − *School of Mechanical Engineering, Beijing Key Laboratory of Pipeline Critical Technology and Equipment for Deepwater Oil & Gas Development, Beijing Institute of Petrochemical Technology, Beijing 102617, China*

Wenquan Tao − *Key Laboratory of Thermo-Fluid Science and Engineering, Ministry of Education, School of Energy & Power Engineering, Xi'an Jiaotong University, Xi'an, Shaanxi 710049, China;* orcid.org/0000-0002-2348-6299

Yu Zou − *School of Mechanical Engineering, Beijing Key Laboratory of Pipeline Critical Technology and Equipment for Deepwater Oil & Gas Development, Beijing Institute of Petrochemical Technology, Beijing 102617, China*

Complete contact information is available at: https://pubs.acs.org/10.1021/acs.langmuir.0c00747

Notes

The authors declare no competing financial interest.

ACKNOWLEDGMENTS

This work is supported by the National Natural Science Foundation of China (Nos. 51936001, 51636006, and 51606012) and the Program of Great Wall Scholar (No. CIT&TCD20180313).

REFERENCES

(1) Mehralizadeh, A.; Shabanian, S. R.; Bakeri, G. Effect of modified surfaces on bubble dynamics and pool boiling heat transfer enhancement: A review. *Therm. Sci. Eng. Prog.* **2020**, *15*, No. 100451.

(2) Balss, K. M.; Avedisian, C. T.; Cavicchi, R. E.; Tarlov, M. J. Nanosecond imaging of microboiling behavior on pulsed-heated au films modified with hydrophilic and hydrophobic self-assembled monolayers. *Langmuir* **2005**, *21*, 10459−10467.

(3) Thomas, O. C.; Cavicchi, R. E.; Tarlov, M. J. Effect of Surface Wettability on Fast Transient Microboiling Behavior. *Langmuir* **2003**, *19*, 6168−6177.

(4) Bourdon, B.; Rioboo, R.; Marengo, M.; Gosselin, E.; De, C. J. Influence of the wettability on the boiling onset. *Langmuir* **2012**, *28*, 1618−24.

(5) Kumar, C. S. S.; Chang, Y. W.; Chen, P. H. Effect of heterogeneous wettable structures on pool boiling performance of cylindrical copper surfaces. *Appl. Therm. Eng.* **2017**, *127*, 1184−1193.

(6) Hsu, C. C.; Lee, M. R.; Wu, C. H.; Chen, P. H. Effect of interlaced wettability on horizontal copper cylinders in nucleate pool boiling. *Appl. Therm. Eng.* **2017**, *112*, 1187−1194.

(7) Sujith, C. S.; Chang, Y.; Arenales, M.; Kuo, L. S.; Chuang, Y.; Chen, P. H. Experimental investigation on the effect of size and pitch of hydrophobic square patterns on the pool boiling heat transfer performance of cylindrical copper surface. *Inventions* **2018**, 3, No. 15.

(8) Wang, C. H.; Dhir, V. K. Effect of surface wettability on active nucleation sited density during pool boiling of water on a vertical surface. *J. Heat Transfer* **1993**, *115*, 659−669.

(9) Bourdon, B.; Bertrand, E.; Di, M. P.; Marengo, M.; Rioboo, R.; De, C. J. Wettability influence on the onset temperature of pool boiling: experimental evidence onto ultra-smooth surfaces. *Adv. Colloid Interface Sci.* **2015**, *221*, 34−40.
(10) Bertossi, R.; Caney, N.; Gruss, J. A.; Poncelet, O. Pool boiling enhancement using switchable polymers coating. *Appl. Therm. Eng.* **2015**, *77*, 121−126.
(11) Ilić, M. M.; Petrović, M. M.; Stevanović, V. D. Boiling heat transfer modelling: a review and future prospectus. *Therm. Sci.* **2019**, *23*, 87−107.
(12) Cao, Q.; Cui, Z. Molecular dynamics simulations of the effect of surface wettability on nanoscale liquid film phase-change. *Numer. Heat Transfer, Part A* **2019**, *75*, 533−547.
(13) Shavik, S. M.; Hasan, M. N.; Morshed, A. K. M. M.; Islam, M. Q. Molecular dynamics study of effect of different wetting conditions on evaporation and rapid boiling of ultra-thin argon layer over platinum surface. *Procedia Eng.* **2015**, *105*, 446−451.
(14) Hens, A.; Agarwal, R.; Biswas, G. Nanoscale study of boiling and evaporation in a liquid Ar film on a Pt heater using molecular dynamics simulation. *Int. J. Heat Mass Transfer* **2014**, *71*, 303−312.
(15) Wang, Y.; Wang, S.; Lu, G.; Wang, X. Effects of wettability on explosive boiling of nanoscale liquid films: Whether the classical nucleation theory fails or not? *Int. J. Heat Mass Transfer* **2019**, *132*, 1277−1283.
(16) Wu, N.; Zeng, L.; Fu, T.; Wang, Z.; Lu, C. Molecular dynamics study of rapid boiling of thin liquid water film on smooth copper surface under different wettability conditions. *Int. J. Heat Mass Transfer* **2020**, *147*, No. 118905.
(17) Yamamoto, T.; Matsumoto, M. Initial stage of nucleate boiling: molecular dynamics investigation. *J. Therm. Sci. Technol.* **2012**, *7*, 334−349.
(18) Chen, Y.; Zou, Y.; Yu, B.; Sun, D.; Chen, X. Effects of surface wettability on rapid boiling and bubble nucleation: a molecular dynamics study. *Nanoscale Microscale Thermophys. Eng.* **2018**, *22*, 198−212.
(19) Chen, Y.; Zou, Y.; Wang, Y.; Han, D.; Yu, B. Bubble nucleation on various surfaces with inhomogeneous interface wettability based on molecular dynamics simulation. *Int. Commun. Heat Mass Transfer* **2018**, *98*, 135−142.
(20) Chen, Y.; Li, J.; Yu, B.; Sun, D.; Zou, Y.; Han, D. Nanoscale study of bubble nucleation on a grooved substrate using molecular dynamics simulation. *Langmuir* **2018**, *34*, 14234−14248.
(21) Zhou, W.; Li, Y.; Li, M.; Wei, J.; Tao, W. Bubble nucleation over patterned surfaces with different wettabilities: Molecular dynamics investigation. *Int. J. Heat Mass Transfer* **2019**, *136*, 1−9.
(22) Nagayama, G.; Tsuruta, T.; Cheng, P. Molecular dynamics simulation on bubble formation in a nanochannel. *Int. J. Heat Mass Transfer* **2006**, *49*, 4437−4443.
(23) Delhommelle, J.; Millie, P. Inadequacy of the Lorentz-Berthelot combining rules for accurate predictions of equilibrium properties by molecular simulation. *Mol. Phys.* **2001**, *99*, 619−625.
(24) Plimpton, S. Fast parallel algorithms for short-range molecular dynamics. *J. Comput. Phys.* **1995**, *117*, 1−19.
(25) Allen, M. P.; Tildesley, D. J.; Banavar, J. R. *Computer Simulation of Liquids*; Oxford University Press: New York, 1987.
(26) Chen, Y.; Yu, B.; Zou, Y.; Chen, B.; Tao, W. Study on the effect of foreign particle on bubble nucleation by using molecular dynamics simulation. *J. Mol. Liq.* **2020**, *305*, No. 112876.
(27) Acharya, H.; Mozdzierz, N. J.; Keblinski, P.; Garde, S. How Chemistry, Nanoscale Roughness, and the Direction of Heat Flow Affect Thermal Conductance of Solid-Water Interfaces. *Ind. Eng. Chem. Res.* **2012**, *51*, 1767−1773.

https://dx.doi.org/10.1021/acs.langmuir.0c00747
Langmuir 2020, 36, 5336−5348